A revisit of drawdown behavior during pumping in unconfined aquifers

Deqiang Mao,[1,2] Li Wan,[1] Tian-Chyi J. Yeh,[2,3] Cheng-Haw Lee,[3] Kuo-Chin Hsu,[3] Jet-Chau Wen,[4] and Wenxi Lu[5]

Received 16 March 2010; revised 7 February 2011; accepted 7 March 2011; published 6 May 2011.

[1] In this study, the S-shaped log-log drawdown-time curve typical of pumping tests in unconfined aquifers is reinvestigated via numerical experiments. Like previous investigations, this study attributes the departure of the S shape from the drawdown-time behavior of the confined aquifer to the presence of an "additional" source of water. Unlike previous studies, this source of water is reinvestigated by examining the temporal and spatial evolution of the rate of change in storage in an unconfined aquifer during pumping. This evolution is then related to the transition of water release mechanisms from the expansion of water and compaction of the porous medium to the drainage of water from the unsaturated zone above the initial water table and initially saturated pores as the water table falls during the pumping of the aquifer. Afterward, the 1-D vertical drainage process in a soil column is simulated. Results of the simulation show that the transition of the water release mechanisms in the 1-D vertical flow without an initial unsaturated zone can also yield the S-shaped drawdown-time curve as in an unconfined aquifer. We therefore conclude that the transition of the water release mechanisms and vertical flow in the aquifer are the cause of the S-shaped drawdown-time curve observed during pumping in an unconfined aquifer. We also find that the moisture retention characteristics of the aquifer material have greater impact than its relative permeability characteristics on the drawdown-time curve. Furthermore, influences of the spatial variability of saturated hydraulic conductivity, specific storage, and saturated moisture content on the drawdown curve in the saturated zone are found to be more significant than those of other unsaturated properties. Finally, a cross-correlation analysis reveals that the drawdown at a location in a heterogeneous unconfined aquifer is mainly affected by local heterogeneity near the pumping and observation wells. Applications of a model assuming homogeneity to the estimation of aquifer parameters as such may require a large number of observation wells to obtain representative parameter values. In conclusion, we advocate that the governing equation for variably saturated flow through heterogeneous media is a more appropriate and realistic model that explains the S-shaped drawdown-time curves observed in the field.

Citation: Mao, D., L. Wan, T.-C. J. Yeh, C.-H. Lee, K.-C. Hsu, J.-C. Wen, and W. Lu (2011), A revisit of drawdown behavior during pumping in unconfined aquifers, *Water Resour. Res.*, *47*, W05502, doi:10.1029/2010WR009326.

1. Introduction

[2] The response of an unconfined aquifer during a pumping test often is characterized by an S-shaped drawdown-time curve on a log-log-scale graph. More specifically, when an unconfined aquifer is pumped at a constant rate, the depth-averaged drawdown appears to follow the *Theis* [1935] solution for flow in a confined aquifer at early times; at intermediate times, the drawdown becomes less than that predicted by the Theis model; the drawdown again appears to conform to the Theis solution at late times. Such a phenomenon has often been referred to as the delayed yield or delayed gravity response of the water table. The explanation and analysis of this response have been a topic for debate over the years.

[3] Flow processes induced by pumping in unconfined aquifers are generally complex because of the presence of saturated and unsaturated zones and the time-varying interface of the two zones (the water table) in addition to the heterogeneous nature of geologic media. As a consequence, hydrologists over the past few decades have adopted simplified conceptual models such that the mathematical analysis

[1]School of Water Resources and Environmental Science, China University of Geosciences, Beijing, China.
[2]Department of Hydrology and Water Resources, University of Arizona, Tucson, Arizona, USA.
[3]Department of Resources Engineering, National Cheng Kung University, Tainan, Taiwan.
[4]Department of Environmental and Safety Engineering, Research Center for Soil and Water Resources and Natural Disaster Prevention, National Yunlin University of Science and Technology, Touliu, Taiwan.
[5]College of Environment and Resources, Jilin University, Changchun, China.

Copyright 2011 by the American Geophysical Union.
0043-1397/11/2010WR009326

of the drawdown caused by pumping in an unconfined aquifer is mathematically tractable.

[4] Generally speaking, two categories of conceptual mathematical models based on analytical solutions have been developed over the years to quantify and explain the delayed yield phenomenon. The first category is the depth-averaged, radial flow model with a delayed drainage source term [*Boulton*, 1954, 1963]. As stated by *Boulton* [1963, p. 470], "the water-bearing material through which the water table has fallen during the early stages of pumping does not yield up its water immediately." As a result, the Boulton model includes an empirical delay coefficient to the specific yield term to represent the slow water release process and to account for the intermediate stage of the S-shaped well hydrograph (the log-log drawdown-time data plot).

[5] The other category includes those based on a concept of instantaneous and complete drainage at the water table [e.g., *Dagan*, 1967; *Brutsaert*, 1970; *Streltsova*, 1972a, 1972b; *Neuman*, 1972; *Lakshminarayana and Rajagopalan*, 1978]. These are radial flow models that consider a 2-D flow field in the vertical plane along the radial distance, and the delayed drawdown region of the drawdown-time curve is considered to be caused by the downward hydraulic head gradient below the water table (i.e., delayed water table response). They neglect the influence of the unsaturated zone above the water table and assume instantaneous drainage of the initially saturated pores.

[6] Application of both types of models to drawdown-time data collected from field pumping tests generally yields specific yield values that are substantially below those that would be expected on the basis of other methods of measurement [see *Nwankwor et al.*, 1984; *Endres et al.*, 2007]. *Nwankwor et al.* [1984] attributed the low values of specific yield obtained from the type curve methods to an inadequate representation of the drainage processes occurring near the water table.

[7] On the basis of the field data, *Nwankwor et al.* [1992] explained the S-shaped drawdown-time behavior of unconfined sand aquifers as a consequence of changes in vertical hydraulic gradients and water content profile above the water table (i.e., expansion of capillary fringe). Numerical modeling of variably saturated flow by *Akindunni and Gillham* [1992] and analysis of drainage from a soil column by *Narasimhan and Zhu* [1993] supported the explanation by *Nwankwor et al.* [1992] about the importance of the initially unsaturated zone above the water table. *Narasimhan and Zhu* [1993] concluded that a simple exponential release function used by *Boulton* [1963] does not accurately simulate drainage from above the water table. To obtain a more general mathematical approximation of the drainage process, *Moench et al.* [2001] developed an analytical model that used a linear combination of exponential functions to simulate release from above the water table.

[8] *Endres et al.* [2007] compared bulk vadose zone responses predicted by the analytical models [e.g., *Boulton*, 1954, 1963; *Neuman*, 1972; *Moench et al.*, 2001] and inferred from field measurements using hydraulic head data and soil moisture content profiles obtained during a 7 day pumping test at Canadian Forces Base Borden, Ontario. They concluded that the water table boundary conditions used in these analytical models do not adequately replicate the mechanisms controlling the vadose zone behavior during a pumping test.

[9] *Tartakovsky and Neuman* [2007] developed a semi-analytical model that includes flow through the unsaturated zone above the water table. The analytical nature of the model forced them to ignore unsaturated flow induced by lowering the water table during the pumping test and to assume that the unsaturated hydraulic conductivity and moisture capacity term vary with elevation instead of capillary pressure, which varies with flow at different locations. On the basis of this model, they concluded that unsaturated flow in the vadose zone above the initial water table has significant impact on dimensionless log-log drawdown-time behavior in the saturated zone when the aquifer has large retention capacity and/or small initial saturated thickness. Moreover, as horizontal saturated hydraulic conductivity increases relative to the vertical, the effect of unsaturated flow on drawdown in the aquifer diminishes.

[10] Although effects of heterogeneity on variably saturated flow have been investigated by *Li and Yeh* [1998], few have investigated the effects of heterogeneity on drawdown-time curves during pumping in unconfined aquifers. *Akindunni and Gillham* [1992] mentioned possible effects of heterogeneity when analyzing data from pumping tests in the Borden aquifer. *Bunn et al.* [2010] conducted a Monte Carlo analysis to investigate the effects of the spatial variability of the saturated hydraulic conductivity in the unconfined aquifer on the capillary fringe extension observed in the field [*Bevan et al.*, 2005].

[11] Previous studies have either implicitly or explicitly related the origin of the S-shaped behavior to the transition of water release mechanisms (from the expansion of water and compaction of the aquifer to the drainage of saturated pores due to the falling of the water table). The exact nature of this behavior, however, has been a source of confusion and debate. For example, concepts like delayed yield and expansion of capillary fringe give the impression that there must be a source of water above the initial water table (unsaturated zone) that acts as a source of recharge. The delayed water table response concept, on the other hand, neglects the unsaturated zone above the water table and assumes instantaneous drainage of the initially saturated pores as the water table falls. Moreover, the effects of heterogeneity on the S-shaped curve remain unknown. In this study, numerical experiments of pumping in an unconfined aquifer are conducted using a finite element numerical model that solves the governing equations for flow through variably saturated media. On the basis of the numerical experiments, we examine the rate of change in storage at various locations in the aquifer, including the saturated zone, the vadose zone above the initial water table, and the porous medium after the lowering of the water table in the aquifer. The S-shaped log-log drawdown-time behavior during pumping in an unconfined aquifer is then related to the transition of the water release mechanism from compaction of porous media and expansion of water to actual dewatering of porous media under vertical flows.

[12] A first-order stochastic moment approach is also developed to quantify the effects of spatial variability of parameters for both saturated and unsaturated zones on the drawdown-time curve induced by the pumping in the aquifer. This paper subsequently uses the stochastic moment approach to explore the role of heterogeneity in the development of the S-shaped drawdown-time curves and the spatial cross correlation between the drawdown at

a given location and heterogeneity at various parts of the aquifer. Finally, implications of the results of this study are discussed.

2. Methodology

[13] A finite element numerical model, Variably Saturated Flow and Transport in 3D (VSAFT3), by *Srivastava and Yeh* [1992] is used in this investigation. This program solves the partial differential equation that describes flow in 3-D, variably saturated geologic media:

$$\nabla \cdot [K(h,\mathbf{x})\nabla(h+z)] = \omega S_s(\mathbf{x})\frac{\partial h}{\partial t} + \frac{\partial \theta}{\partial t} = [\omega S_s(\mathbf{x}) + C(h,\mathbf{x})]\frac{\partial h}{\partial t}, \tag{1}$$

where ∇ is the spatial gradient, t is time, θ represents the volumetric moisture content, z is the elevation, which is positive upward, and h is the pressure head and is positive when the medium is fully saturated and negative when unsaturated. The saturation index ω is equal to 1 if the medium is saturated and 0 if the medium is unsaturated. The term $S_s(\mathbf{x})$ represents the specific storage, $C(h, \mathbf{x})$ is the soil moisture capacity, which can be derived from the moisture-pressure constitutive relationship, and $K(h, \mathbf{x})$ is the hydraulic conductivity-pressure constitutive function. The program uses the Newton-Raphson iteration scheme to solve the nonlinear finite element approximation of equation (1).

[14] We use VSAFT3 to simulate flow to a well due to pumping in a 3-D unconfined aquifer. The aquifer is 200 × 200 m in the horizontal plane and 9 m in the vertical and is discretized into 380,880 finite elements. A variable mesh is used for the discretization. In the vertical plane, a vertical interval of 0.2 m is used from z = 6.0 to 7.5 m (i.e., about the water table) and a vertical interval of 0.5 m is used from z = 0.0 to 6.0 m and from z = 7.5 to 9.0 m. In the horizontal plane, the interval of the mesh is 0.5 m from x = 76 to 124 m and y = 76 to 124 m (around the pumping well) and is 4.0 m otherwise.

[15] A no-flux boundary is assigned to the top (no infiltration or evaporation) and bottom of the aquifer; no-flux boundaries are imposed on the other four sides of the aquifer. The initial pressure head distribution in the aquifer is set to be hydrostatic, with the water table at z = 6.7 m representing a static condition. A well is represented by a line source of length 4.0 m from the bottom center of the aquifer (x = 100 m, y = 100 m) with a constant rate of discharge (0.06 m^3/min), in which the borehole storage is neglected.

[16] The hydraulic conductivity–pressure head and moisture–pressure head constitutive relationship of the aquifer are described by an exponential model [*Gardner*, 1958]:

$$K(h) = K_s \exp(\alpha h), \tag{2}$$

$$\theta(h) = \theta_r + (\theta_s - \theta_r)\exp(\beta h), \tag{3}$$

respectively. In equations (2) and (3), α and β are pore size distribution parameters for the unsaturated hydraulic conductivity–pressure head function and the moisture–pressure head relationship, respectively; θ_s and θ_r denote saturated and residual water content. Note that $(\theta_s - \theta_r)$is equivalent to the specific yield in previous studies of aquifer tests.

[17] For the cases where the aquifer is assumed to be homogeneous, values of the parameters in equations (2) and (3) are taken from the study by *Akindunni and Gillham* [1992]: K_s = 0.00396 m/min, S_s = 0.000325/m, θ_s = 0.37, θ_r = 0.07, α = 4.0/m, and β = 4.0/m. The thickness of the capillary fringe (or air entry value) is assumed to be $1/\beta$. The pumping test is simulated for 2000 min.

[18] In order to investigate the effect of parameter heterogeneity on the drawdown-time curve, a first-order stochastic moment analysis developed by *Li and Yeh* [1998] and *Hughson and Yeh* [2000] is used. Specifically, natural logarithms of the parameters in the constitutive relationships of the unsaturated hydraulic properties are treated as stochastic processes in space, which are characterized by their means and spatial covariance functions. Subsequently, the head is expanded in a Taylor series about the mean values of hydraulic parameters. After neglecting the second-order and high-order terms, the first-order approximation of the total head can be written as

$$\begin{aligned} H(\mathbf{x},t) = \overline{H}(\mathbf{x},t) + p(\mathbf{x},t) = \overline{H}(\mathbf{x},t) + f(\mathbf{x})\frac{\partial H}{\partial \ln K_S(\mathbf{x})} \\ + s(\mathbf{x})\frac{\partial H}{\partial \ln S_S(\mathbf{x})} + a(\mathbf{x})\frac{\partial H}{\partial \ln \alpha(\mathbf{x})} + b(\mathbf{x})\frac{\partial H}{\partial \ln \beta(\mathbf{x})} \\ + t_s(\mathbf{x})\frac{\partial H}{\partial \ln \theta_s(\mathbf{x})} + t_r(\mathbf{x})\frac{\partial H}{\partial \ln \theta_r(\mathbf{x})}, \end{aligned} \tag{4}$$

where $f(\mathbf{x})$, $s(\mathbf{x})$, $a(\mathbf{x})$, $b(\mathbf{x})$, $t_s(\mathbf{x})$, and $t_r(\mathbf{x})$ are the perturbations of the logarithms of parameters, $K_s(\mathbf{x})$, $S_s(\mathbf{x})$, $\alpha(\mathbf{x})$, $\beta(\mathbf{x})$, $\theta_s(\mathbf{x})$, and $\theta_r(\mathbf{x})$, respectively. These perturbations are dimensionless. $\overline{H}$ is the mean total head, evaluated using the mean parameters, and it represents the head in an equivalent homogeneous aquifer; p denotes the head perturbation around the mean head, resulting from spatial variability of the parameters. The partial derivatives are the sensitivity matrices, which are evaluated at the mean parameters $\overline{K_s}$, $\overline{S_s}$, $\overline{\alpha}$, $\overline{\beta}$, $\overline{\theta_s}$, and $\overline{\theta_r}$. According to equation (4), the head perturbation can be written in a matrix form as

$$\mathbf{p} = \mathbf{J}_{pf}\mathbf{f} + \mathbf{J}_{ps}\mathbf{s} + \mathbf{J}_{pa}\mathbf{a} + \mathbf{J}_{pb}\mathbf{b} + \mathbf{J}_{pt_s}\mathbf{t}_s + \mathbf{J}_{pt_r}\mathbf{t}_\mathbf{r}. \tag{5}$$

Here bold symbols denote either matrices or vectors. $\mathbf{J}_{pf}$ is the sensitivity of $\mathbf{p}$ to change in parameter $\boldsymbol{f}$ or Jacobian matrix, which is calculated by the adjoint method [see *Sykes et al.*, 1985; *Li and Yeh*, 1998, 1999; *Hughson and Yeh*, 2000]. Multiplying equation (5) with itself, taking the expectation, and assuming that the perturbation of the different parameters are statistically independent from each other lead to the covariance of the head:

$$\begin{aligned} \mathbf{R}_{pp} = \mathbf{J}_{pf}\mathbf{R}_{ff}\mathbf{J}_{pf}^T + \mathbf{J}_{ps}\mathbf{R}_{ss}\mathbf{J}_{ps}^T + \mathbf{J}_{pa}\mathbf{R}_{aa}\mathbf{J}_{pa}^T + \mathbf{J}_{pb}\mathbf{R}_{bb}\mathbf{J}_{pb}^T \\ + \mathbf{J}_{pt_s}\mathbf{R}_{t_st_s}\mathbf{J}_{pt_s}^T + \mathbf{J}_{pt_r}\mathbf{R}_{t_rt_r}\mathbf{J}_{pt_r}^T. \end{aligned} \tag{6}$$

$\mathbf{R}_{ff}$, $\mathbf{R}_{ss}$, $\mathbf{R}_{aa}$, $\mathbf{R}_{bb}$, $\mathbf{R}_{t_st_s}$, and $\mathbf{R}_{t_rt_r}$ are the covariance function matrices for the parameters, which are assumed to follow an exponential covariance model [*Gelhar*, 1993]. The superscript T denotes the transpose. Each diagonal element of $\mathbf{R}_{pp}$ is the head variance σ_p^2 at location $\mathbf{x}$ and at time t, representing the mean-square deviation of the head in a heterogeneous aquifer from the head calculated using the mean parameters for the homogeneous aquifer. The corresponding standard deviation σ_p is added to and subtracted from mean drawdown-time curves at a given observation location calculated

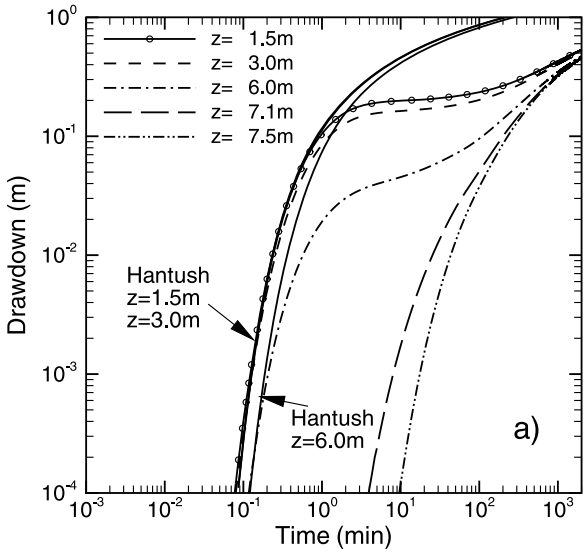

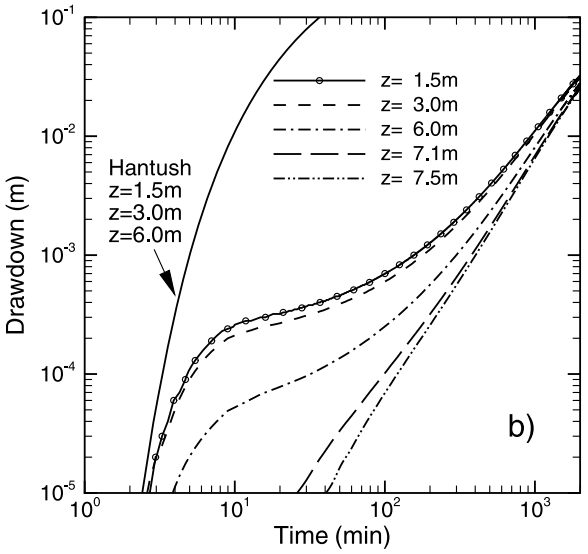

Figure 1. Log-log drawdown-time curves at five different elevations (z = 1.5, 3.0, 6.0, 7.1, and 7.5 m) at (a) r = 5 m and (b) r = 30 m. Solid lines denote the results based on the solution by Hantush at three observation elevations in the saturated zone, z = 1.5, 3.0, and 6.0 m. In Figure 1a, the difference between the Hantush solution at z = 1.5 m and z = 3.0 m is not distinguishable. In Figure 1b, the solutions are the same at all three elevations.

by the mean parameters to yield upper and lower bounds of the drawdown-time curve. Such lower and upper bounds delineate the influence of heterogeneity of different parameters. In other words, the log-log drawdown-time curve of a heterogeneous unconfined aquifer will likely fall in between these bounds. Greater differences between the upper and lower bounds suggest that the log-log drawdown-time curve of the heterogeneous aquifer may be quite different from the perfect S shape obtained using the mean parameters, representing an equivalent homogeneous aquifer. While the first-order analysis only yields approximate upper and lower bounds and Monte Carlo simulations with a large number of realizations would produce more accurate upper and lower bounds, the result of the first-order analysis efficiently illustrates the general effects of heterogeneity on the S-shaped drawdown-time curve.

[19] To evaluate the mean head in equation (4), the values of the mean parameters are assumed to be the same as the parameter values in the homogeneous case, and VSAFT3 is used. Two levels of heterogeneity (variances of the logarithm of parameters equal to 0.1 and 1) for all parameters are examined. In addition, the spatial structure of all parameters is assumed to be described by a 3-D exponential correlation function with some specified correlation scales in the horizontal and vertical directions, which represent the spatial structure of the heterogeneity.

[20] In addition to the first-order stochastic moment analysis, a single realization of each parameter field is generated using a stochastic field generator with the given mean and variance and correlation scales of the parameters of the exponential constitutive model. These fields are then input to VSAFT3 to simulate the response of a heterogeneous aquifer. The response of the heterogeneous aquifer is subsequently compared to the response derived from mean parameters (homogeneous aquifer) to show the effect of heterogeneity on the drawdown-time curve.

[21] Subsequently, a cross-correlation analysis is carried out to investigate how the head at a given location in the saturated zone is affected by the parameter value at different locations in the aquifer. This cross-correlation analysis again is based on the first-order stochastic moment analysis. For example, the cross correlation between p at location $\mathbf{x}_i$ and f at $\mathbf{x}_j$ can be expressed as

$$\rho_{pf}(\mathbf{x}_i, \mathbf{x}_j, t) = \frac{\mathbf{R}_{pf}(\mathbf{x}_i, \mathbf{x}_j, t)}{\sigma_p(\mathbf{x}_i, t)\sigma_f} = \frac{\mathbf{J}_{pf}(\mathbf{x}_i, \mathbf{x}_j, t)\mathbf{R}_{ff}(\mathbf{x}_i, \mathbf{x}_j)}{\sigma_p(\mathbf{x}_i, t)\sigma_f}, \qquad (7)$$

where j = 1, N, with N being the total number of elements in the domain, and σ_f is the standard deviation of f. Here we also assume independence of each different parameter. The cross correlation between p at location $\mathbf{x}_i$ and the other parameters at $\mathbf{x}_j$ can be written in a similar expression.

3. Results and Discussions

[22] The results and discussions will be grouped into (1) flow to a well in a homogeneous aquifer, (2) 1-D variably saturated flow, and (3) flow to a well in a heterogeneous aquifer.

3.1. Flow to a Well in a Homogeneous Aquifer

3.1.1. Drawdown-Time Curve

[23] Simulated drawdowns in the unconfined aquifer as a function of time at five elevations (1.5, 3.0, 6.0, 7.1, and 7.5 m) at radial distances of 5.0 and 30.0 m from the pumping well are plotted using log scales in Figures 1a and 1b, respectively. Note that elevations 7.1 and 7.5 m are above the water table, and drawdowns at these elevations denote the change of pressures in the vadose zone due to pumping in the saturated zone. Figure 1 shows that drawdowns in the saturated zone exhibit the characteristic S shape, which is most pronounced at the bottom of the aquifer. The flat part of the S curve at z = 6.0 m occurs earlier than at the bottom of the aquifer (i.e., z = 1.5 m and z = 3.0 m). On the other hand, the drawdown-time curves at elevations 7.1 and 7.5 m in the

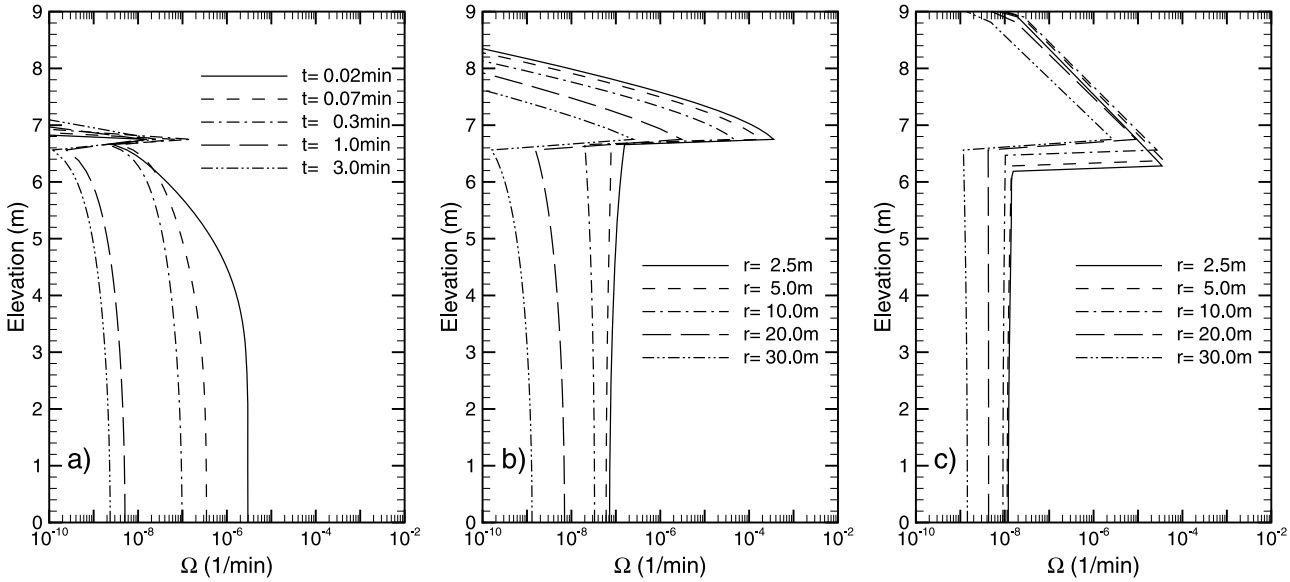

Figure 2. Ω as a function of elevation (a) at five early times (t = 0.02, 0.07, 0.3, 1.0, and 3.0 min) corresponding to five different radii (r = 2.5, 5, 10, 20 and 30 m), (b) at an intermediate stage (10 min after pumping), and (c) at a late stage (1000 min after pumping) at the five radii. The water table is located at the sharp discontinuity.

unsaturated zone do not exhibit the S shape. These simulated results are consistent with field observations [e.g., *Bevan et al.*, 2005].

[24] Figures 1a and 1b also show drawdown-time curves at different elevations (z = 1.5, 3.0, and 6.0 m) in a confined aquifer that has an infinite lateral extent, with the same saturated thickness (6.7 m) and the saturated hydraulic properties of the unconfined aquifer. These curves are obtained by using the solution of *Hantush* [1961a, 1961b], which considers the partial perforation of the pumping well in the aquifer. According to Figure 1a, drawdowns in the confined aquifer at r = 5 m at higher elevation z = 6.0 m are smaller that those at z = 1.5 m and z = 3.0 m, which is indicative of vertical flow. At r = 30.0 m, far from the pumping well, identical drawdowns at the three elevations suggest that the effect of the partial perforation of the pumping well (i.e., vertical flow) is negligible (Figure 1b). As expected, no S-shaped curve is observed.

[25] Note that in both Figures 1a and 1b the drawdown-time curves in the unconfined aquifer depart from their initial steep drawdown portion and deviate from the corresponding drawdowns of the confined aquifer in a descending elevation order (i.e., z = 6.0 m, z = 3.0 m, and z = 1.5 m). This sequential departure (i.e., smaller drawdowns than the confined aquifer) implies that an apparent "additional" source of water is flowing from the upper to the lower part of the saturated zone of the aquifer as recharge, in comparison with the flow process in the confined aquifer. As will be explained in section 3.1.2, such an "additional" source of water is mainly attributed to a different water release mechanism at this stage of the flow process in the unconfined aquifer as opposed to delayed yield or expansion of the capillary fringe mechanism proposed by previous studies.

3.1.2. Rate of Change in Storage

[26] Different from previous works, our study uses the evolution of the "rate of change in storage" per volume of the porous medium Ω at various distances and depths during a pumping test in an unconfined aquifer to explain the so-called "delayed yield" phenomenon. Mathematically, this rate of change in storage is the right-hand side of equation (1), which represents the net mass flux in a unit volume of the porous medium:

$$\Omega = [\omega S_s(\mathbf{x}) + C(h, \mathbf{x})] \frac{\partial h}{\partial t}. \tag{8}$$

In VSAFT3, each node links a number of elements depending on the discretization. The rate of change in storage per unit volume around a node between two successive time steps is calculated by dividing the change in storage over the elements associated with the node by the time step and total volume of the elements.

3.1.3. Early Times

[27] In Figure 2a, the quantity Ω is plotted as a function of elevation at different radial distances from the pumping well at various times of the early stage of the S-shaped drawdown-time curve. Specifically, these distances and times are r = 2.5 m at t = 0.02 min, r = 5.0 m at t = 0.07 min, r = 10 m at t = 0.3 min, r = 20 m at t = 1.0 min, and r = 30 m at t = 3.0 min. We use different times for different radii to illuminate the effect. At this early stage, the Ω value at r = 2.5 m is the largest at the bottom of the aquifer over the elevation from 0 to 4 m where the pumping well screen is located. This value then decreases with elevation and reaches the minimum at the water table; it then increases sharply at the water table and subsequently decreases with elevation in the unsaturated zone. Overall, the Ω values below the water table exhibit a strong nonlinear pattern with greater Ω values at the bottom of the aquifer than those near the water table. This pattern is consistent with the fact that the greatest change in pressure is at the bottom of the aquifer near the pumping location. The Ω value in the unsaturated zone at these times is virtually zero except close to the water table. Similar behaviors are also observed at the other radial distances. As pointed out in

previous studies, this behavior suggests that water flow into the pumping well is mainly from expansion of water and compaction of the aquifer in the saturated zone, which is characterized by the specific storage of the aquifer. This time period corresponds to the early time segment in the log-log drawdown-time plot. The water table position can only be approximated from the plot of Ω as a function of elevation in Figure 2, as different finite element meshes are used at different radial distances.

3.1.4. Intermediate Times

[28] During the intermediate stage (the flat portion) of the log-log drawdown-time curve ($t = 10$ min after pumping), the behavior of Ω as a function of elevation at $r = 2.5$, 5.0, 10.0, 20.0, and 30.0 m from the pumping well is shown in Figure 2b. In comparison with Figure 2a, the Ω values in the vadose zone above the water table (near the sharp break in curve around $z = 6.5$ m) at all radii begin to increase. The Ω values in the saturated region below the water table decrease at all radial distances. The closer to the pumping well the location is, the greater the reduction in Ω is in comparison with Figure 2a. Furthermore, the Ω values at locations close to the pumping well are almost constant with elevation. All these behaviors indicate that the flow field near the well is close to the steady state (quasi-steady state) in which the head field changes at the same rate at all elevations.

[29] Figure 2b also suggests that pumping has begun to induce a significant amount of water to be released from the vadose zone to supply the well discharge, whereas the elastic storage of the aquifer near the pumping location is almost exhausted. In other words, the drainage of water from pores in the unsaturated zone increasingly becomes the primary source of water for the well discharge. It yields more water to the saturated region below than the elastic storage of the region itself and contributes to an "additional" source of water compared with the similar flow in the confined aquifer. As a result, the drawdown-time curve deviates from that based on the Hantush solution [*Hantush*, 1961a, 1961b]. The transition of the water release mechanism from compaction of the porous medium and expansion of water to dewatering of pores thus describes the "additional" source of water and, in turn, the flat part of the intermediate stage of the S-shaped drawdown-time curve. This is consistent with the importance of the initial vadose zone brought forth by *Nwankwor et al.* [1992], *Akindunni and Gillham* [1992], and *Narasimhan and Zhu* [1993].

3.1.5. Late Times

[30] The behavior of Ω as a function of elevation at the five radii at $t = 1000$ min after pumping (i.e., the late stage of the S curve) is plotted in Figure 2c. At this stage the water table at all radii starts to fall noticeably; the Ω values in the unsaturated zone are much greater at high elevations at this late stage than the early or the intermediate stage. The Ω values in the saturated region at all radii are very small and do not vary with the elevation. These behaviors of the Ω values indicate that flow in this region apparently approaches steady state conditions; water released from the unsaturated zone and from previously saturated pores due to the falling of the water table is equal to the amount of water withdrawn by the pumping well. Thus, little change in storage occurs in the saturated region of the aquifer. Note that although there is still water released from the aquifer due to compaction of the aquifer and expansion of water, its amount is much smaller than the amount of water released from falling of the water table and the initially unsaturated zone.

3.2. One-Dimensional Vertical Variably Saturated Flow

[31] To further emphasize the importance of the transition of the water release mechanism from compaction of the aquifer to drainage of porous media in the formation of the S-shaped hydrograph, the drainage process of a vertical soil column is simulated. The column is 150 cm in length and 0.1 cm in width and thickness. The column is discretized into 1500 square elements that are 0.1 cm in length, width, and thickness. Such a small element size is selected to ensure accurate tracking of the location of the water table and the correct mass balance of the experiments.

[32] No-flux boundaries are assigned to the top, bottom, and sides of the column. The initial pressure distribution in the domain is assumed to be hydrostatic. The initial water table is located at an elevation of 110 cm from the bottom of the vertical domain, and the initial thickness of the unsaturated zone is 40 cm. At time greater than zero, a constant discharge $q = 0.08$ cm/min is imposed at the bottom boundary of the column. The simulation lasts 150 min, and drawdown data (difference between the initial head and head after the drainage starts) are recorded at elevations $z = 10$, 40, 70 cm.

[33] The saturated hydraulic parameters for the soil column are $K_s = 0.495$ cm/min, $S_s = 0.0001$/cm. The experiment is conducted for two different unsaturated hydraulic properties: the exponential model (equations (2) and (3)) and the *van Genuchten* [1980] model:

$$\theta(h) = \theta_r + (\theta_s - \theta_r)(1 + \gamma|h|^n)^{-m}, \tag{9}$$

where vertical bars indicate absolute value, θ_s is the saturated moisture content, θ_r is the moisture content at residual saturation, and γ, n, and m are shape-fitting parameters, with $m = 1 - 1/n$. We further assume that $K(h)$ follows *Mualem*'s [1976] pore size distribution model, which is expressed as

$$K(h) = \frac{K_s\left\{1 - (\gamma|h|)^{n-1}[1 + (\gamma|h|)^n]^{-m}\right\}^2}{[1 + (\gamma|h|)^n]^{m/2}} \tag{10}$$

where K_s is the locally isotropic saturated hydraulic conductivity and γ, n, and m are assumed to be the same as those in equation (9). Hereafter, equations (9) and (10) are referred to as the VGM model. The parameters for the exponential model are $\alpha = 0.25$/cm, $\beta = 0.15$/cm, $\gamma = 0.15$/cm, and $n = 2.5$ for the VGM model. For both models, θ_s and θ_r are set to 0.35 and 0.045, respectively. Note that the VGM model has a slightly more distinct capillary fringe than the exponential model.

[34] An analytical solution describing saturated flow in a semi-infinite vertical domain [*Ozisik*, 1993] is also used to describe drawdown behavior due to the release of water from the column caused by compaction of the porous medium and expansion of water only. Using the definition of hydraulic diffusivity $D = K/S_s$, the analytical solution to the governing equation,

$$\frac{\partial^2 H}{\partial z^2} = \frac{1}{D}\frac{\partial H}{\partial t}, \tag{11}$$

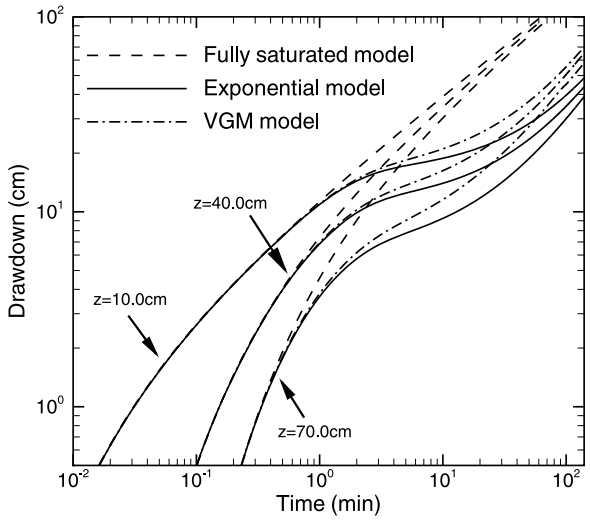

Figure 3. Comparison of drawdown-time curves at three different elevations, z = 10 cm, z = 40 cm, and z = 70 cm, in a fully saturated column with those in a soil column with an unsaturated zone of 40 cm with the exponential constitutive relationships and with those with VGM constitutive relationships.

with initial and boundary conditions,

$$H|_{t=0} = H_0, \quad K\left.\frac{\partial H}{\partial z}\right|_{z=0} = q, \quad H|_{z=\infty} = H_0, \tag{12}$$

is

$$s(z,t) = H_0 - H = H_0 - \frac{q}{K} \cdot \left\{ 2\sqrt{\frac{Dt}{\pi}}\exp\left(-\frac{z^2}{4Dt}\right) - z\left[1 - \mathrm{erf}\left(\frac{z}{2\sqrt{Dt}}\right)\right]\right\}, \tag{13}$$

where $s(z, t)$ is the drawdown. The parameters and discharge in equation (13) are kept the same as those in the 1-D variably saturated experiment, i.e., K_s = 0.495 cm/min, S_s = 0.0001/cm, and q = 0.08 cm/min.

[35] Figure 3 depicts simulated drawdowns as a function of time at elevations z = 10 cm, z = 40 cm, and z = 70 cm during the drainage process in the soil column with the exponential and the VGM models as well as during the drainage process under the fully saturated condition. According Figure 3, 1-D vertical variably saturated flow can yield S-shaped log-log drawdown-time curves similar to those drawdown-time curves in the 3-D unconfined aquifer. Furthermore, the drawdown from the variably saturated model deviates from the drawdown of the fully saturated model sequentially, at z = 70 cm first, then at z = 40 cm, and then at z = 10 cm. This sequential occurrence of the deviation (smaller drawdown) indicates that the water released by desaturation of the unsaturated zone above the water table arrives at z = 70 cm first and then progressively migrates downward. In other words, the transition of water release mechanism progresses from the location near the water table to the bottom of the column. These results are the same as those in the case of pumping in an unconfined aquifer indicated in Figure 1.

[36] The overall shapes of the drawdown-time curves resulting from the two models are similar. Drawdowns based on the VGM model are, however, consistently larger than those based on the exponential model once the effects of the drainage process become effective. This can be attributed to the greater water-holding capacity of the moisture retention curve of the VGM model. These results suggest that the use of the VGM or the exponential model does not significantly change the result in general. Therefore, the exponential model will be used in the rest of analysis.

[37] The Ω values in the 1-D vertical column as a function of elevation at t = 0.01, 3.0, and 100.0 min after drainage started are plotted in Figure 4a. At the early time (t = 0.01 min), change in storage takes place below the water table; it is the greatest at the bottom of the column, and it decreases nonlinearly toward zero near the elevation of 50 cm. The discharge from the column at this time is the water released because of compaction of the porous medium and expansion of the water. At t = 3.0 min, the nonlinear behavior of the Ω value in the saturated zone becomes less pronounced; contributions from the unsaturated zone above the water table begin to increase. The sharp decrease in the rate of change in storage occurs at the location corresponding to the water table. Above the water table, the rate of change in storage decreases nonlinearly with height. At time equal to 100 min, the water table has dropped significantly. The rate of change in storage of the unsaturated zone above the water table becomes very large. Conversely, the Ω values at all locations below the water table become very small and remain constant over the depth, indicating that flow in the saturated zone below the water table is close to a steady state. That is, discharge from desaturation of previously saturated pores because of the falling of the water table and desaturation of the unsaturated zone above are transmitted to the bottom discharge boundary without causing a noticeable change in storage in the region below the water table. At this time, the discharge from the column is mainly from the drainage of pores above the water table. Note that the behavior of the Ω value in the 1-D experiment is very similar to that in the 3-D experiments (Figure 2).

[38] Figure 4b depicts the cumulative volume of water released over the length of the column as a function of time. The volume of water released is classified into three groups: (1) from compaction of the aquifer, (2) from drainage of the unsaturated zone above the initial water table and (3) from drainage of the initially saturated medium during falling of the water table. Figure 4b illustrates the relative importance of each group at different times of the S-shaped curve in Figure 3.

3.2.1. Effects of the Hydraulic Conductivity Curve Versus the Moisture Retention Curve

[39] The comparison of the simulated drawdown-time curves based on the VGM and the exponential models indicates that the moisture-pressure constitutive relation seems to have a greater influence on the drawdown than the hydraulic conductivity–pressure constitutive relation. To confirm this speculation, the 1-D column drainage problem is investigated with the exponential model with different α and β. The parameter α dictates the rate of reduction in unsaturated hydraulic conductivity, while β controls the rate of reduction in moisture content as the medium becomes less saturated. Figures 5a and 5b illustrate the influence of parameters α and β, respectively, on the log-log drawdown-time

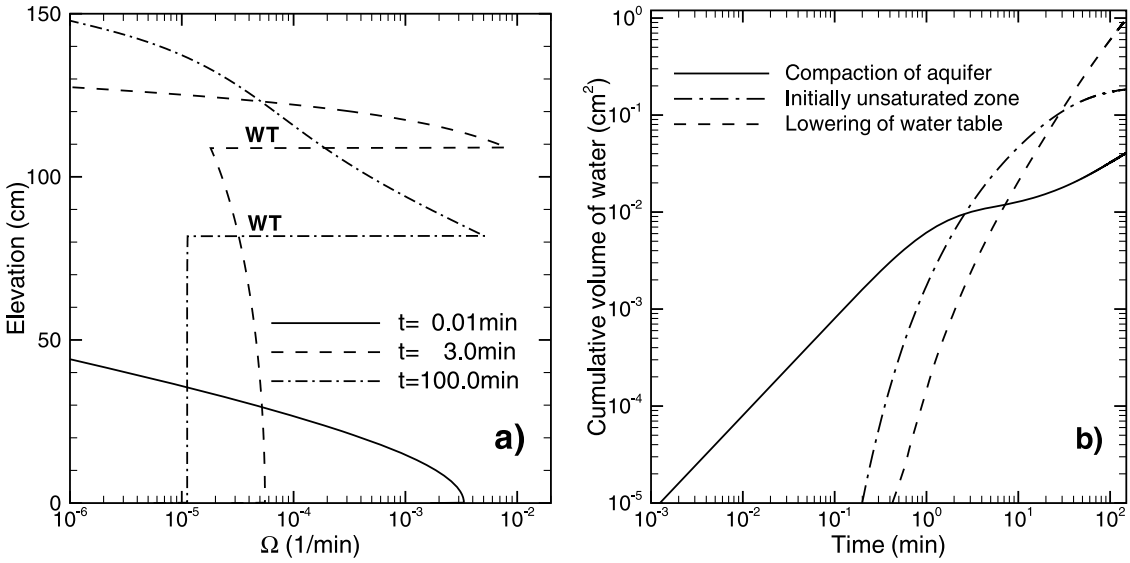

Figure 4. (a) Rate change in storage Ω as a function of the elevation in a 1-D soil column for exponential model at times of 0.01, 3.0, and 100 min after drainage started. WT denotes the water table. The initial water table before draining is at 110 cm. (b) Cumulative volume of water released from (1) compaction of the aquifer, (2) drainage from the initial unsaturated zone, and (3) drainage from pores during falling of the water table over the column at a function of time.

behavior at elevation z = 20 cm in the column. With an increase in the value of α, drawdown becomes greater, and the S shape of the drawdown-time curve becomes less obvious. Conversely, when the value of β increases, the drawdown becomes smaller, and the S shape becomes more pronounced. That is, a porous medium that has a smaller air entry value (a large β value) in the moisture retention curve can release more water from pores than a medium with a larger air entry value (a small β value). This finding is consistent with the previous findings of the effects of the exponential and VGM models on the S-shaped drawdown-time curve. As indicated by these results, the influence of the two parameters on drawdown is entirely different. Therefore, it is inappropriate to treat these two parameters as identical, as has been done in the past [e.g., *Tartakovsky and Neuman*, 2007]. In effect, laboratory experiments by *Yeh and Harvey* [1990] and *Moench* [2008] have demonstrated that the two parameters are not necessarily the same.

3.2.2. Role of an Initially Unsaturated Zone

[40] While the important role of the vadose zone (initially unsaturated zone) has been emphasized by many previous studies, as discussed in section 1, our study here advocates the importance of transition of the water release mechanisms in variably saturated flow process during an aquifer pumping test. That is, we argue that even in a fully saturated aquifer without an initially unsaturated zone, the transition between the two water release mechanisms may occur when the discharge is greater than recharge, and thus, initially fully saturated pores are desaturated. As such, S-shaped drawdown curves likely will occur during pumping in such an aquifer.

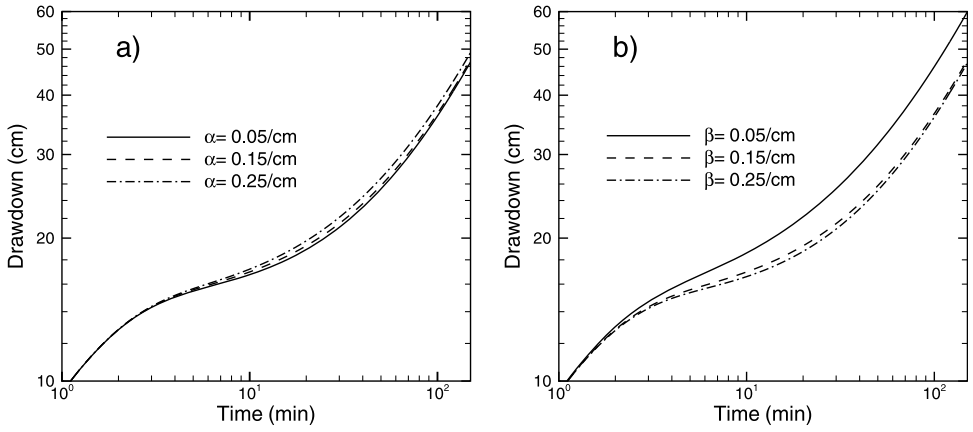

Figure 5. Drawdown-time curve at z = 20 cm with (a) different α values when β = 0.15/cm and (b) different β values while fixing α = 0.15/cm.

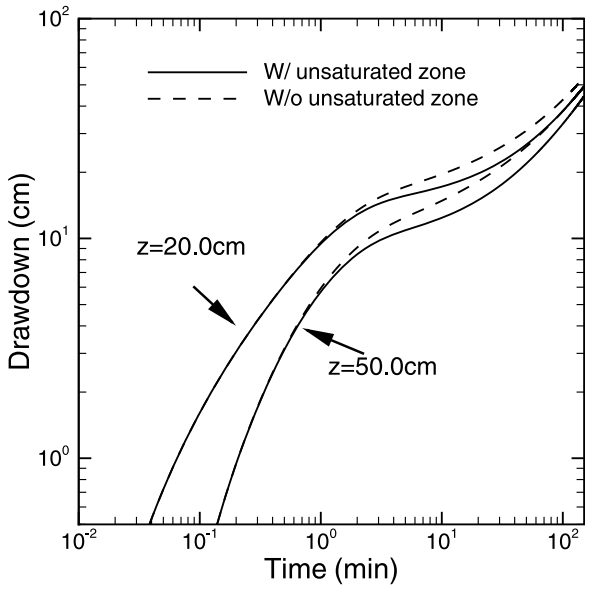

Figure 6. Drawdown-time curve at two elevations, $z = 20$ and 50 cm, showing the role of an initial unsaturated zone.

[41] In order to test this hypothesis, we conducted a new numerical column experiment by relocating the upper impermeable boundary to the location of the initial water table of the previous column experiment. As a result, the length of the new column is reduced to 110 cm from the length of 150 cm of the previous experiment. The new column is initially fully saturated, with a hydrostatic pressure head distribution with zero pressure at the top. We shall call the previous experiment case 1, which involves the vadose zone, and the new experiment case 2, in which the vadose zone does not exist. Figure 6 shows the log-log drawdown-time curves at two elevations (z = 20 and 50 cm) for the two cases. In both cases, the log-log drawdown-time curves follow an S shape. At the beginning, the drawdown curves are identical for the two cases because the water is released strictly from the specific storage of the column of the two cases. Afterward, water is released mainly from the unsaturated zone and desaturation of the initially fully saturated pores because of the falling of the water table for case 1. On the other hand, in case 2, water is released mainly from the latter. While log-log drawdown-time curves of both cases are similar, a major difference between the two cases is that for the case without an initial unsaturated zone, the drawdown is slightly greater because no water from initially unsaturated zone is available as in case 1. At large times, behaviors of the two drawdown-time curves appear to be the same, although the drawdown in case 2 is slightly higher.

[42] Results of this experiment further confirm that the "additional" source of water causing the S-shaped drawdown curve is not limited to the additional water from the initial vadose zone above the water table of an unconfined aquifer. It also includes the drainage of initially fully saturated pores in the saturated zone. Therefore, the transition of the water release mechanism during vertical flows is the cause of the S-shaped drawdown observed in the saturated zone during pumping in an unconfined aquifer. The concept of the expansion of capillary fringe proposed by *Nwankwor et al.* [1992] and the delayed yield concept are phenomena created by this transition of water release mechanisms.

3.3. Flow to a Well in Heterogeneous Aquifers

3.3.1. Drawdown-Time Curve

[43] As mentioned in section 2, the effects of spatial variability of aquifer parameters on the drawdown-time curve will be quantified by an upper bound and a lower bound of the drawdown around its mean as a function of time at an observation point in the aquifer. The upper bound is the mean drawdown plus the standard deviation of the head σ_p at the given time and location, and the lower bound is the mean minus σ_p.

[44] The mean drawdown-time curves for the aquifer considered have been presented in Figure 1. The temporal evolution of σ_p at three elevations, $z = 3$, 6, and 7.1 m, at radius $r = 5$ m from the pumping well in the aquifer due to the spatial variability of all six hydraulic parameters (K_s, S_s, α, β, θ_s, and θ_r) is plotted as solid red lines in Figures 7a–7c. The three elevations represent the bottom, the middle of the saturated zone, and the initially unsaturated zone of the unconfined aquifer. The contributions to σ_p from the variability of each of the six parameters are shown as lines with different symbols in the same plot. Similar plots for locations at $r = 30$ m at elevations $z = 3$, 6, and 7.1 m are illustrated in Figures 7d, 7e, and 7f, respectively. The aquifer considered in Figures 7d–7f is statistically isotropic with a correlation scale of 3 m in all directions. The variances of the logarithm of parameters are intentionally set to the same variance, 1.0, so that the effect of the variance can be isolated.

[45] According to Figures 7a and 7d, the head standard deviation in the initially unsaturated zone (note that initial water table is located at $z = 6.7$ m) at $r = 5$ m and $r = 30$ m generally increases with time. However, it decreases slightly at the location close to pumping well ($r = 5$ m, Figure 7a) at large times. This reduction can be attributed to the fact that the flow in the unsaturated zone close to the well approaches the hydrostatic condition earlier. Overall, variations in K_s and θ_s are shown to have greater effects on the head variation in the unsaturated zone than α, β, and θ_r, and the effect of the variation in S_s is minimal.

[46] For the head in the saturated region, the impact of the variation in K_s is the most profound, and it persists over time (see Figures 7b, 7c, 7e, and 7f). The effect of variability in S_s is as significant as that of K_s at the early time, but it decreases rapidly and stabilizes when the transition of the water release mechanism from elastic compaction and expansion to the drainage of pores commences or when the variability of unsaturated parameters (α, β, θ_s, and θ_r) takes effect. At large times, the effects of the variability of θ_s become as significant as those of K_s and greater than the effects of the variability of α, β, and θ_r.

[47] Comparisons of Figures 7a–7c with Figures 7d–7f indicate that the temporal evolution of the head standard deviation due to the variability of each parameter at the same elevation at different radii from the pumping well follows similar patterns. In the saturated zone, the head standard deviation increases rapidly at the early time, stabilizes slightly at the intermediate time, and increases again at the large time (Figures 7b, 7c, 7e, and 7f). This seems to suggest that the head standard deviation is dependent on the mean hydraulic head. The magnitude of the head standard deviation generally is smaller at a larger distance ($r = 30$ m) from the pumping well.

[48] In general, smaller variances of the parameters are found to yield a smaller σ_p, while the temporal evolution of σ_p

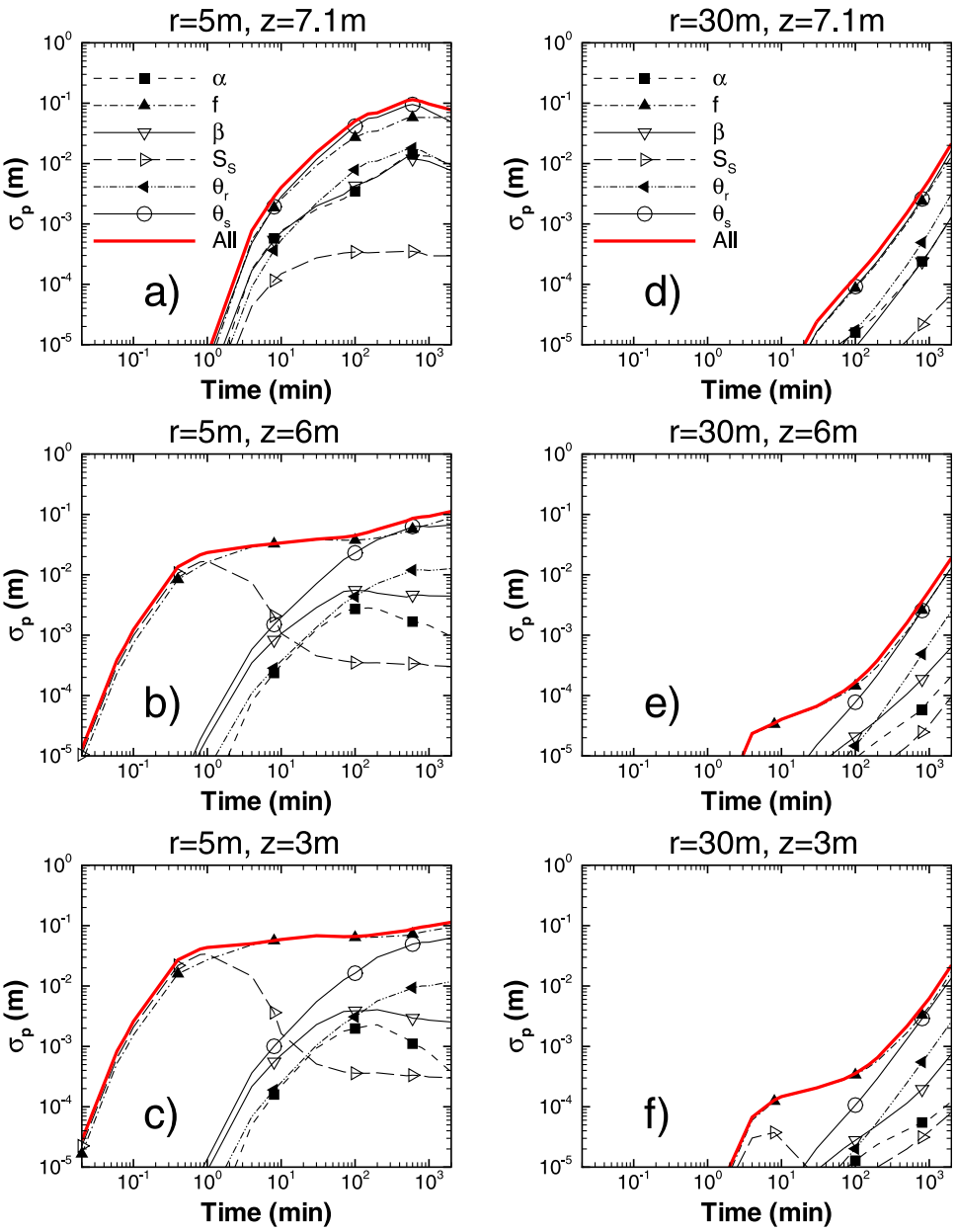

Figure 7. Standard deviation σ_p of the head for every parameter as a function of time with variances of 1.0 and correlation scale of 3 m. (a–f) Results for the observation point at two different radii, r = 5 and 30 m, and three different elevations, z = 3, 6, and 7.1 m. The red solid lines show the combined effect of all six parameters.

remains the same as those shown in Figure 7. Similarly, as the statistical anisotropy increases (i.e., the correlation scales in the horizontal directions become greater than the vertical one), the magnitude of σ_p increases, and the temporal behavior of σ_p remains similar to those of aquifers with statistical isotropy (Figure 7). This implies that the effects of variability of parameters on the head increase if the geologic formation is stratified.

[49] The above analysis shows that even if the variance of the logarithm of parameters is assumed to be the same, the variability of K_s, S_s, or θ_s has greater impact on the drawdown-time curve in the saturated zone than the variability of α, β, and θ_r. While few studies have quantified the variance of the parameters of the exponential model, studies of the variance of the VGM parameters at several field sites [*Russo and Bouton*, 1992] have shown that the variability of the parameters for saturated media is generally greater than that of parameters for unsaturated media. Therefore, the spatial variability of parameters of media under unsaturated conditions does not have significant impact on the drawdown-time curve in the saturated zone during pumping tests in unconfined aquifers. These results may also suggest that identifying the spatial variability of the α and β values of the exponential model for the vadose zone using the head observed in the saturated zone may be difficult unless head and moisture content measurements in the unsaturated zone are used.

[50] To demonstrate the utility of the head standard deviation, a single realization of heterogeneous unconfined

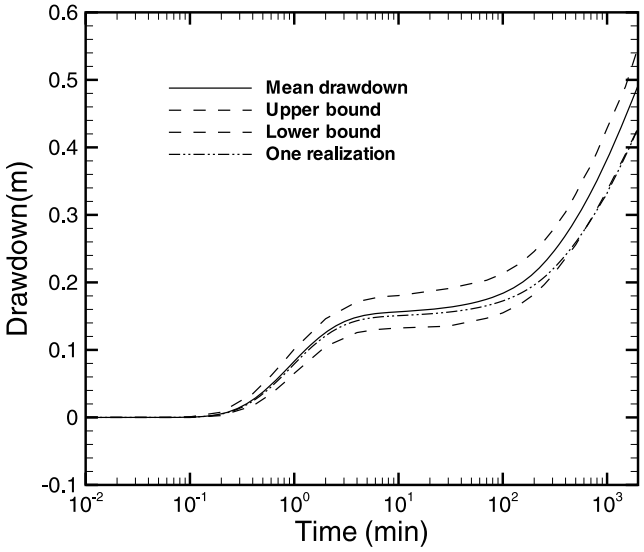

Figure 8. Deviations of the drawdown-time curve in an aquifer with heterogeneous K_s, S_s, and θ_s (variance of ln K_s, ln S_s, and ln θ_s is 0.25, 0.25, and 0.05, respectively) from the drawdown-time curve derived with the assumption of aquifer homogeneity. The upper and lower bounds based on the first-order stochastic moment analysis that quantify the deviation are also shown.

aquifers is created. In this example, we consider only the combined effects of the spatial variability of K_s, S_s, and θ_s because other parameters have minor impact on the drawdown, as indicated in Figure 7. To make this example realistic, vertical and horizontal correlation scales of the heterogeneity are set to be 0.15 and 3.0 m, respectively, the same as the statistics of the Borden aquifer [see *Sudicky*, 1986]. The variance for K_s is specified as 0.25 according to the work by *Woodbury and Sudicky* [1991], and the same is true for S_s. A variance of 0.05 is assigned for θ_s. The mean values of these parameters, pumping rate, and setup are the same as the values used in the previous 3-D homogeneous model.

[51] Figure 8 shows the simulated drawdown as a function of time at $r = 5$ m and $z = 3$ m in this heterogeneous aquifer, the corresponding mean drawdown-time curve predicted on the basis of the aquifer homogeneity assumption, and upper and lower bounds associated with the mean curve. Apparently, the drawdown-time curve of this realization of heterogeneous aquifers is different from the one based on a homogeneous model using the mean parameter values and is bounded by its upper and lower bounds. In other words, the upper and lower bounds are a measure of uncertainty associated with prediction based on the homogeneous model (or likely deviation of drawdown in a heterogeneous aquifer from the predicted one assuming aquifer homogeneity). The deviation reported by *Akindunni and Gillham* [1992] of the observed drawdown in the Borden aquifer from that predicted by an equivalent homogeneous model thus is likely due to local heterogeneity neglected by the model. That is, one should not force an equivalent homogenous model to reproduce exactly the observed drawdown-time curve in a field aquifer. The upper and lower bounds can serve as the calibration target to avoid overfitting of the model.

3.3.2. Cross-Correlation Analysis

[52] The degree of influence on the head at a given location in the aquifer by different properties at every part of the aquifer of the above example at different times is discussed next. Figure 9 shows the spatial distributions of the cross-correlation value between the head observed at $r = 5$ m and $z = 3$ m and K_s in a cross-sectional vertical plane running through the pumping well and the observation location. At the early time (0.08 min), when the water table remains static, the head at the observation location is negatively correlated with K_s values in the region between the pumping well and the observation location (Figure 9a). At the intermediate time ($t = 10$ min), when the water table starts to fall, the head becomes positively correlated with K_s in the area above the observation point and the pumping well and is negatively correlated with K_s in the region between the observation location and pumping well, below the positive correlation zone (Figure 9b). This pattern of correlation (from the upper positive correlation region to the negative correlation region) follows the direction of the vertical flow. This intermediate time period corresponds to the time when the flat portion of the drawdown-time curve occurs (Figure 1). At the large time (1000 min), the lowering of the water table near the pumping well becomes noticeable. The positive correlation region at $t = 10$ min breaks into two: one at the top left of the observation and the other to the right of the pumping well (Figure 9c). Such changes in the correlation pattern seem to follow the change of the flow field (i.e., from mostly vertical flow to greater horizontal flow). The overall nonsymmetrical pattern is consistent with results from *Mizell et al.* [1982], *Li and Yeh* [1999], *Wu et al.* [2005], and *Zhu and Yeh* [2006] for confined aquifers. That is, the head at a given location is positively correlated with K_s of the up-gradient region and negatively correlated with K_s in the down-gradient region with respect to the head location along the streamline toward the pumping well. It is slightly positively correlated with K_s along streamlines on the other side of the pumping well.

[53] Similar to previous studies [*Wu et al.*, 2005], positive correlation values between the head and S_s field are found to be confined to a narrow region between the pumping and the observation location at early times (Figure 10); this correlation diminishes to zero as flow near the pumping well approaches a quasi steady state during the late times.

[54] A very small positive cross correlation of the observed head and θ_s appears at the early time $t = 10$ min and is confined to the region above the observation location and the water table. This positive correlation then continues to increase, and the size of the correlated area expands with the expansion of cone of depression as time progresses (Figure 11). That is, the head at the observation location at the late time is highly influenced by the θ_s values in this region.

[55] These results demonstrate that the drawdown at an observation location in the aquifer is not equally influenced by heterogeneity everywhere in the aquifer. Such a finding thus raises the same salient question about the representativeness of the estimates using models that assume homogeneity and a limited number of observations, as done by *Wu et al.* [2005]. *Wu et al.* [2005], *Straface et al.* [2007], and *Wen et al.* [2010] demonstrated that estimated effective T and S of an equivalent homogeneous, confined aquifer based on a limited number of observations vary with the locations of

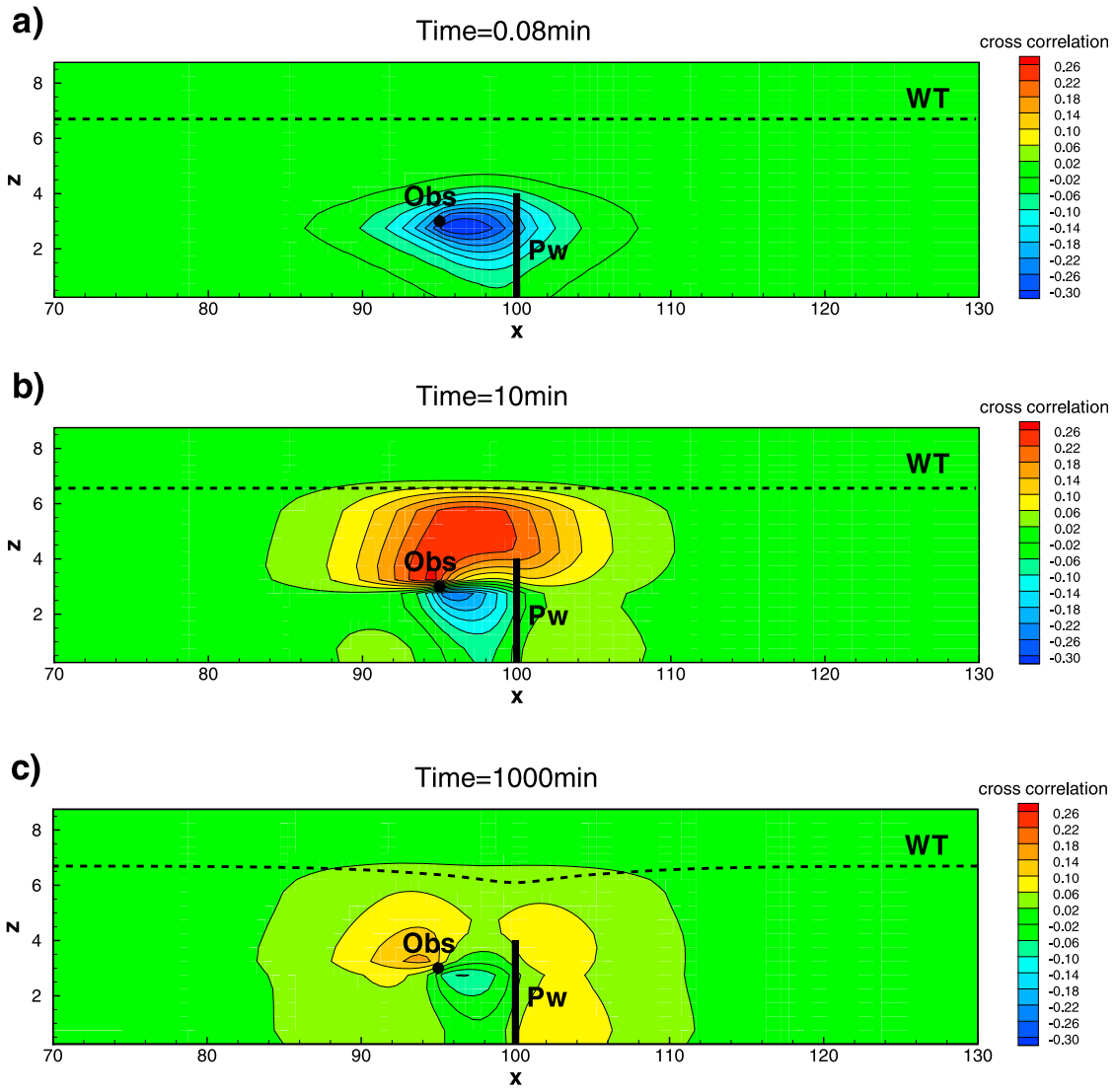

Figure 9. Spatial distributions of the cross correlation between the head at the observation point (Obs, $x = 95.0$ m, $y = 100.0$ m, and $z = 3.0$ m) and K_s along a vertical plane running through both the pumping well (Pw) and the observation point at (a) the early time, (b) the intermediate time, and (c) the late time of an S-shaped drawdown-time curve.

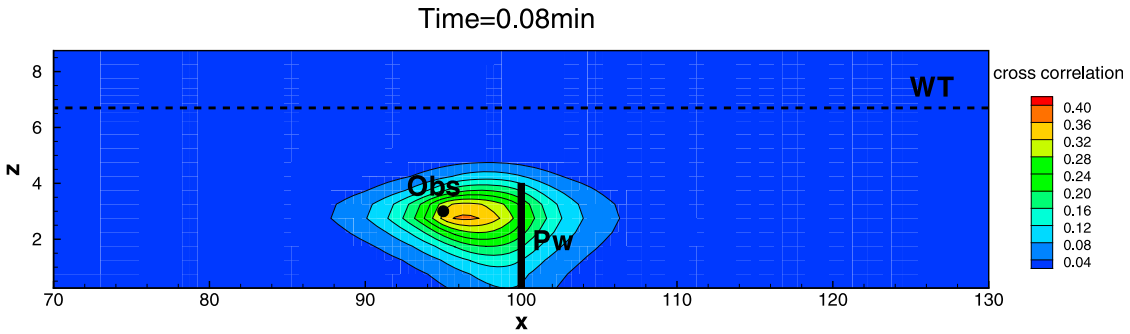

Figure 10. Spatial distributions of the cross correlation between the head at the observation point (Obs, $x = 95.0$ m, $y = 100.0$ m, and $z = 3.0$ m) and S_s along a vertical plane running through both the pumping well (Pw) and the observation point at the early time of an S-shaped drawdown-time curve. The cross correlation diminishes as the time progresses.

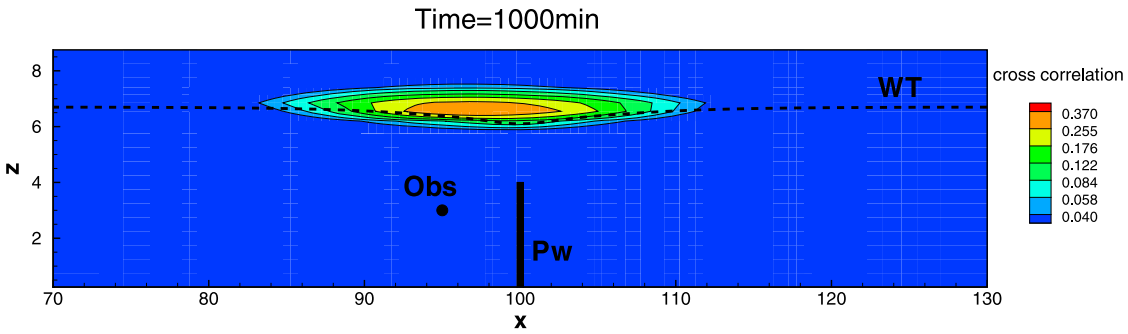

Figure 11. Spatial distributions of the cross correlation between the head at the observation point (Obs, $x = 95.0$ m, $y = 100.0$ m, and $z = 3.0$ m) and along a vertical plane running through both the pumping well (Pw) and the observation point at the late time of an S-shaped drawdown-time curve.

pumping and observation wells. Likewise, the estimated T anisotropy of the equivalent homogeneous aquifer varies in magnitude and direction unless a large number of observation wells are used such that the ergodicity assumption (i.e., equivalence of ensemble and spatial average) embedded in the homogeneous flow equations is satisfied. We believe the same issues confront the estimation of parameters for unconfined aquifers by application of a model based on the homogeneity assumption without using a large number of observation wells [e.g., *Tartakovsky and Neuman*, 2007]. These issues certainly deserve a rigorous analysis, which is, however, beyond the scope of this paper.

[56] Finally, results of our analysis point to a simple fact: A multidimensional variably saturated flow model such as equation (1), which considers the transition of water release mechanisms and heterogeneity, would provide a more realistic representation of flow processes in the unconfined aquifer during a pumping test. In addition, our results show that the variability of unsaturated constitutive relationships in the unsaturated zone does not significantly influence the head in the saturated zone except θ_s, which does not vary significantly in general. As a result, recently developed hydraulic tomography [*Gottlieb and Dietrich*, 1995; *Vasco et al.*, 2000; *Yeh and Liu*, 2000; *Bohling et al.*, 2002; *Liu et al.*, 2002; *Brauchler et al.*, 2003; *Zhu and Yeh*, 2005, 2006; *Li et al.*, 2007; *Liu et al.*, 2007; *Illman et al.*, 2007, 2008; *Fienen et al.*, 2008; *Castagna and Bellin*, 2009; *Cardiff et al.*, 2009; *Yin and Illman*, 2009; *Xiang et al.*, 2009; *Illman et al.*, 2010] coupled with equation (1) using spatially averaged unsaturated constitutive relationships for the unsaturated zone (i.e., neglecting their spatial variability) may foster a practical way for delineating K_s and S_s heterogeneity in the saturated region of the unconfined aquifer.

4. Conclusion

[57] Previous studies have either implicitly or explicitly related the S-shaped behavior to transition in water release mechanisms. Nevertheless, the exact nature of this behavior has been a source of debate. For example, concepts like delayed yield and the expansion of capillary fringe give the impression that an unsaturated zone above the water table that acts as a "source of recharge" must exist. Our analysis shows that a transition in water release mechanisms during vertical flow in a soil column produces the S-shaped behavior even in the absence of an initial unsaturated zone. The delayed water table response concept, on the other hand, omits the influence of the unsaturated zone above the water table and assumes instantaneous drainage of the initially saturated pores. Our study of the rate of change in storage at various locations in the aquifer shows that an initial unsaturated zone above the water table is important, and the drainage of the initially saturated pores is continuous in space and time as the water table falls. We believe the widely accepted terms "delayed yield," which indicates a lag in water release from the initially unsaturated zone, and "delayed water table response" do not elucidate the transition of the two water release mechanisms, and perhaps these terms are misleading.

[58] The first-order stochastic moment analysis shows that the S-shaped drawdown-time curve during a pumping test in unconfined aquifers is sensitive to the spatial variability of hydraulic conductivity, specific storage, and saturated moisture content and is insensitive to the variability of other parameters for unsaturated hydraulic properties. Nevertheless, the average unsaturated hydraulic properties of the aquifer are important. In order to identify the average unsaturated hydraulic properties, measurements of negative pressure heads and moisture contents above the water table are necessary during the pumping test. Furthermore, a cross-correlation analysis reveals that an observed drawdown at a given location in a heterogeneous unconfined aquifer is mainly influenced by local heterogeneity near the pumping and observation wells. As a consequence, applications of a model assuming homogeneity to the estimation of parameters may require a large number of spatial observations in order to yield representative parameter values. This requirement of a large number of observations in space may support an inverse modeling effort to estimate the spatially distributed parameters.

[59] In conclusion, we believe a multidimensional variably saturated flow model, which considers the transition of water release mechanisms and accounts for heterogeneity, would provide a more realistic representation of the flow processes in an unconfined aquifer during a pumping test. Hydraulic tomography would be a viable approach for delineating heterogeneity in unconfined aquifers.

[60] **Acknowledgments.** This research is supported in part by a subcontract from University of Waterloo Canada through a grant from SERDP and NSF grant EAR-1014594. The first author acknowledges the support of "China Scholarship Council." The support from National Cheng-Kung University, Taiwan, National Yunlin University of Science and Technology, Taiwan, and Jiling University, Jilin, China are also acknowledged.

References

Akindunni, F. F., and R. W. Gillham (1992), Unsaturated and saturated flow in response to pumping of an unconfined aquifer: Numerical investigation of delayed drainage, *Ground Water*, *30*, 873–884, doi:10.1111/j.1745-6584.1992.tb01570.x.

Bevan, M. J., A. L. Endres, D. L. Rudolph, and G. Parkin (2005), A field scale study of pumping-induced drainage and recovery in an unconfined aquifer, *J. Hydrol.*, *315*, 52–70, doi:10.1016/j.jhydrol.2005.04.006.

Bohling, G. C., X. Zhan, J. J. Butler Jr., and L. Zheng (2002), Steady shape analysis of tomographic pumping tests for characterization of aquifer heterogeneities, *Water Resour. Res.*, *38*(12), 1324, doi:10.1029/2001WR001176.

Boulton, N. S. (1954), Unsteady radial flow to a pumped well allowing for delayed yield from storage, *Int. Assoc. Sci. Hydrol. Publ.*, *2*, 472–477.

Boulton, N. S. (1963), Analysis of data from nonequilibrium pumping tests allowing for delayed yield from storage, *Proc. Inst. Civ. Eng.*, *26*, 469–482, doi:10.1680/iicep.1963.10409.

Brauchler, R., R. Liedl, and P. Dietrich (2003), A travel time based hydraulic tomographic approach, *Water Resour. Res.*, *39*(12), 1370, doi:10.1029/2003WR002262.

Brutsaert, W. (1970), Immiscible multiphase flow in ground water hydrology: A computer analysis of the well flow problem, Ph.D. thesis, Colo. State Univ., Fort Collins.

Bunn, M. I., J. P. Jones, A. L. Endres, and D. L. Rudolph (2010), Effects of hydraulic conductivity heterogeneity on vadose zone response to pumping in an unconfined aquifer, *J. Hydrol.*, *387*, 90–104, doi:10.1016/j.jhydrol.2010.03.036.

Cardiff, M., W. Barrash, P. K. Kitanidis, B. Malama, A. Revil, S. Straface, and E. Rizzo (2009), A potential-based inversion of unconfined steady-state hydraulic tomography, *Ground Water*, *47*(2), 259–270, doi:10.1111/j.1745-6584.2008.00541.x.

Castagna, M., and A. Bellin (2009), A Bayesian approach for inversion of hydraulic tomographic data, *Water Resour. Res.*, *45*, W04410, doi:10.1029/2008WR007078.

Dagan, G. A. (1967), Method of determining permeability and effective porosity of unconfined anisotropic aquifers, *Water Resour. Res.*, *3*(4), 1059–1071, doi:10.1029/WR003i004p01059.

Endres, A. L., J. P. Jones, and E. A. Bertrand (2007), Pumping-induced vadose zone drainage and storage in an unconfined aquifer: A comparison of analytical model predictions and field measurements, *J. Hydrol.*, *335*, 207–218, doi:10.1016/j.jhydrol.2006.07.018.

Fienen, M. N., T. Clemo, and P. K. Kitanidis (2008), An interactive Bayesian geostatistical inverse protocol for hydraulic tomography, *Water Resour. Res.*, *44*, W00B01, doi:10.1029/2007WR006730.

Gardner, W. R. (1958), Some steady-state solutions of unsaturated moisture flow equations with application to evaporation from a water table, *Soil Sci.*, *85*, 228–232, doi:10.1097/00010694-195804000-00006.

Gelhar, L. W. (1993), *Stochastic Subsurface Hydrology*, Prentice Hall, Englewood Cliffs, N. J.

Gottlieb, J., and P. Dietrich (1995), Identification of the permeability distribution in soil by hydraulic tomography, *Inverse Probl.*, *11*, 353–360, doi:10.1088/0266-5611/11/2/005.

Hantush, M. S. (1961a), Drawdown around a partially penetrating well, *J. Hydraul. Div. Am. Soc. Civ. Eng.*, *87*(HY4), 83–98.

Hantush, M. S. (1961b), Aquifer tests on partially penetrating wells, *J. Hydraul. Div. Am. Soc. Civ. Eng.*, *87*(HY5), 171–194.

Hughson, D. L., and T.-C. J. Yeh (2000), An inverse model for three-dimensional flow in variably saturated porous media, *Water Resour. Res.*, *36*(4), 829–839, doi:10.1029/2000WR900001.

Illman, W. A., X. Liu, and A. Craig (2007), Steady-state hydraulic tomography in a laboratory aquifer with deterministic heterogeneity: Multi-method and multiscale validation of hydraulic conductivity tomograms, *J. Hydrol.*, *341*(3–4), 222–234, doi:10.1016/j.jhydrol.2007.05.011.

Illman, W. A., A. J. Craig, and X. Liu (2008), Practical issues in imaging hydraulic conductivity through hydraulic tomography, *Ground Water*, *46*(1), 120–132.

Illman, W. A., J. Zhu, A. J. Craig, and D. Yin (2010), Comparison of aquifer characterization approaches through steady state groundwater model validation: A controlled laboratory sandbox study, *Water Resour. Res.*, *46*, W04502, doi:10.1029/2009WR007745.

Lakshminarayana, V., and S. P. Rajagopalan (1978), Type-curve analysis of time-drawdown data for partially penetrating wells in unconfined anisotropic aquifers, *Ground Water*, *16*, 328–333, doi:10.1111/j.1745-6584.1978.tb03245.x.

Li, B., and T.-C. J. Yeh (1998), Sensitivity and moment analyses of head in variably saturated regimes, *Adv. Water Resour.*, *21*, 477–485, doi:10.1016/S0309-1708(97)00011-0.

Li, B., and T.-C. J. Yeh (1999), Cokriging estimation of the conductivity field under variably saturated flow conditions, *Water Resour. Res.*, *35*(12), 3663–3674, doi:10.1029/1999WR900268.

Li, W., A. Englert, O. A. Cirpka, J. Vanderborght, and H. Vereecken (2007), Two-dimensional characterization of hydraulic heterogeneity by multiple pumping tests, *Water Resour. Res.*, *43*, W04433, doi:10.1029/2006WR005333.

Liu, S., T.-C. J. Yeh, and R. Gardiner (2002), Effectiveness of hydraulic tomography: Sandbox experiments, *Water Resour. Res.*, *38*(4), 1034, doi:10.1029/2001WR000338.

Liu, X., W. A. Illman, A. J. Craig, J. Zhu, and T.-C. J. Yeh (2007), Laboratory sandbox validation of transient hydraulic tomography, *Water Resour. Res.*, *43*, W05404, doi:10.1029/2006WR005144.

Mizell, S., A. Gutjahr, and L. Gelhar (1982), Stochastic analysis of spatial variability in two-dimensional steady groundwater flow assuming stationary and nonstationary heads, *Water Resour. Res.*, *18*(4), 1053–1067, doi:10.1029/WR018i004p01053.

Moench, A. F. (2008), Analytical model and numerical analyses of unconfined aquifer test considering unsaturated zone characteristics, *Water Resour. Res.*, *44*, W06409, doi:10.1029/2006WR005736.

Moench, A. F., S. P. Garabedian, and D. R. LeBlanc (2001), Estimation of hydraulic parameters from an unconfined aquifer test conducted in a glacial outwash deposit, Cape Cod, Massachusetts, *U.S. Geol. Surv. Prof. Pap.*, *1629*.

Mualem, Y. (1976), A new model for predicting the hydraulic conductivity of unsaturated porous media, *Water Resour. Res.*, *12*(3), 513–522.

Narasimhan, T. N., and M. Zhu (1993), Transient flow of water to a well in an unconfined aquifer: Applicability of some conceptual models, *Water Resour. Res.*, *29*(1), 179–191, doi:10.1029/92WR01959.

Neuman, S. P. (1972), Theory of flow in unconfined aquifers considering delayed response of the water table, *Water Resour. Res.*, *8*(4), 1031–1044, doi:10.1029/WR008i004p01031.

Nwankwor, G. I., J. A. Cherry, and R. W. Gillham (1984), A comparative study of specific yield determinations for a shallow sand aquifer, *Ground Water*, *22*, 764–772, doi:10.1111/j.1745-6584.1984.tb01445.x.

Nwankwor, G. I., R. W. Gillham, G. van der Kamp, and F. F. Akindunni (1992), Effect of the capillary fringe during pumping of unconfined aquifers: Field evidence of delayed drainage, *Ground Water*, *30*(5), 690–700, doi:10.1111/j.1745-6584.1992.tb01555.x.

Ozisik, M. N. (1993), *Heat Conduction*, 2nd ed., John Wiley, New York.

Russo, D., and M. Bouton (1992), Statistical analysis of spatial variability in unsaturated flow parameters, *Water Resour. Res.*, *28*, 1911–1925, doi:10.1029/92WR00669.

Srivastava, R., and T.-C. J. Yeh (1992), A three-dimensional numerical model for water flow and transport of chemically reactive solute through porous media under variably saturated conditions, *Adv. Water Resour.*, *15*(5), 275–287, doi:10.1016/0309-1708(92)90014-S.

Straface, S., T.-C. J. Yeh, J. Zhu, S. Troisi, and C. H. Lee (2007), Sequential aquifer tests at a well field, Montalto Uffugo Scalo, Italy, *Water Resour. Res.*, *43*, W07432, doi:10.1029/2006WR005287.

Streltsova, T. D. (1972a), Unsteady radial flow in an unconfined aquifer, *Water Resour. Res.*, *8*(4), 1059, doi:10.1029/WR008i004p01059.

Streltsova, T. D. (1972b), Unconfined aquifer and slow drainage, *J. Hydrol.*, *16*, 117–124, doi:10.1016/0022-1694(72)90117-5.

Sudicky, E. A. (1986), A natural gradient experiment on solute transport in a sand aquifer: Spatial variability of hydraulic conductivity and its role in the dispersion process, *Water Resour. Res.*, *22*(13), 2069–2082, doi:10.1029/WR022i013p02069.

Sykes, J.-F., J. L. Wilson, and R. W. Andrews (1985), Sensitivity analysis of steady state groundwater flow using adjoint operators, *Water Resour. Res.*, *21*(3), 359–371, doi:10.1029/WR021i003p00359.

Tartakovsky, G. D., and S. P. Neuman (2007), Three-dimensional saturated-unsaturated flow with axial symmetry to a partially penetrating well in a compressible unconfined aquifer, *Water Resour. Res.*, *43*, W01410, doi:10.1029/2006WR005153.

Theis, C. V. (1935), The relation between the lowering of the piezometric surface and the rate and duration of discharge of a well using groundwater storage, *Eos Trans. AGU*, *16*, 519–524.

van Genuchten, M. T. (1980), A closed-form equation for predicting the hydraulic conductivity of unsaturated soils, *Soil Sci. Soc. Am. J.*, *44*, 892–898, doi:10.2136/sssaj1980.03615995004400050002x.

Vasco, D. W., H. Keers, and K. Karasaki (2000), Estimation of reservoir properties using transient pressure data: An asymptotic approach, *Water Resour. Res.*, *36*(12), 3447–3465, doi:10.1029/2000WR900179.

Wen, J. C., C. M. Wu, T.-C. J. Yeh, and C. M. Tseng (2010), Estimation of effective aquifer hydraulic properties from an aquifer test with multi-well observations, *Hydrogeol. J.*, *18*(5), 1143–1155, doi:10.1007/s10040-010-0577-1.

Woodbury, A. D., and E. A. Sudicky (1991), The geostatistical characteristics of the Borden aquifer, *Water Resour. Res.*, *27*(4), 533–546, doi:10.1029/90WR02545.

Wu, C.-M., T.-C. J. Yeh, J. Zhu, T. H. Lee, N.-S. Hsu, C.-H. Chen, and A. F. Sancho (2005), Traditional analysis of aquifer tests: Comparing apples to oranges?, *Water Resour. Res.*, *41*, W09402, doi:10.1029/2004WR003717.

Xiang, J., T.-C. J. Yeh, C.-H. Lee, K.-C. Hsu, and J.-C. Wen (2009), A simultaneous successive linear estimator and a guide for hydraulic tomography analysis, *Water Resour. Res.*, *45*, W02432, doi:10.1029/2008WR007180.

Yeh, T.-C. J., and D. J. Harvey (1990), Effective unsaturated hydraulic conductivity of layered sands, *Water Resour. Res.*, *26*, 1271–1279, doi:10.1029/89WR03638.

Yeh, T.-C. J., and S. Liu (2000), Hydraulic tomography: Development of a new aquifer test method, *Water Resour. Res.*, *36*(8), 2095–2105, doi:10.1029/2000WR900114.

Yin, D., and W. A. Illman (2009), Hydraulic tomography using temporal moments of drawdown recovery data: A laboratory sandbox study, *Water Resour. Res.*, *45*, W01502, doi:10.1029/2007WR006623.

Zhu, J., and T.-C. J. Yeh (2005), Characterization of aquifer heterogeneity using transient hydraulic tomography, *Water Resour. Res.*, *41*, W07028, doi:10.1029/2004WR003790.

Zhu, J., and T.-C. J. Yeh (2006), Analysis of hydraulic tomography using temporal moments of drawdown recovery data, *Water Resour. Res.*, *42*, W02403, doi:10.1029/2005WR004309.

K.-C. Hsu and C.-H. Lee, Department of Resources Engineering, National Cheng Kung University, Tainan, 701, Taiwan.

W. Lu, College of Environment and Resources, Jilin University, Changchun, Jilin, 130026, China.

D. Mao and T.-C. J. Yeh, Department of Hydrology and Water Resources, University of Arizona, Tucson, AZ 85721, USA. (deqiang@email.arizon.edu)

L. Wan, School of Water Resources and Environmental Science, China University of Geosciences, Beijing, 100086, China.

J.-C. Wen, Department of Environmental and Safety Engineering, Research Center for Soil and Water Resources and Natural Disaster Prevention, National Yunlin University of Science and Technology, Touliu, Yunlin, 64045, Taiwan.